 https://doi.org/10.3311/PPme.22389

Periodica Polytechnica Mechanical Engineering, 67(3), pp. 204–213, 2023

Parameter Study of a Loss Reducing Passive Flow Control Method in a Square-to-square Sudden Expansion

Eszter Lukács[1*], János Vad[1]

[1] Department of Fluid Mechanics, Faculty of Mechanical Engineering, Budapest University of Technology and Economics, Műegyetem rkp. 3., H-1111 Budapest, Hungary
[*] Corresponding author, e-mail: lukacs.eszter@gpk.bme.hu

Received: 12 April 2023, Accepted: 20 July 2023, Published online: 31 July 2023

Abstract

The energy consumption of mechanical ventilation in buildings needs to be reduced. An efficient way to achieve this goal is to reduce the hydraulic resistance of the ventilation duct system elements, for example, that of sudden expansions. Ventilation ducts and pipe fittings are frequently of rectangular cross-section. The present paper investigates a passive flow control method in order to reduce the loss coefficient of a square-to-square sudden expansion, where the loss-reducing appendages are short guide vanes, termed as miniflaps, placed at the step edge of the sudden expansion. The turbulent flow is examined numerically using the generalized *k-ω* model of the Ansys Fluent software for different area ratios of the sudden expansion, miniflap lengths, and miniflap angle setups. The Reynolds number is kept constant at $1.08 \cdot 10^5$. Based on the results of the numerical simulations, the loss coefficient of the sudden expansion can be reduced by ~20–25% for an optimum miniflap angle between 9° and 12°. Increasing the length of the miniflaps leads to a greater reduction of the loss coefficient up to a miniflap length of 0.3 d_{h1}, where d_{h1} is the upstream hydraulic diameter of the duct.

Keywords

square duct, sudden expansion, loss reduction, CFD, GEKO

1 Introduction

Pipe systems provide a highly effective way of transporting fluids, such as water, oil, or even fresh air. All elements of these systems – straight pipe sections, elbows, junctions, and area changes – exhibit a flow resistance, which is directly related to the pumping power of the applied machinery to maintain the prescribed mass flow rate in the pipe system. Due to the importance of environmental awareness and the swift increase in the price of energy, hydraulic research has reappeared in the focus of researchers' attention. Among the various hydraulic systems, distinctive attention has been given to mechanical ventilation systems, being more and more indispensable in the building sector and representing a considerable share (~10–20%) [1] of the total energy consumption of edifices. The research in the field of mechanical ventilation is also interesting from the point of view that ventilation ducts are often of rectangular cross-section, which are generally underrepresented in the scientific literature compared to pipes of circular cross-sections.

Hydraulic elements of ventilation duct systems – besides straight ducts – can be categorized into three main groups:

1. change the direction of the flow (elbows, bends);
2. divide or unite the flow (T-junctions, manifolds);
3. change the cross-section of the flow (contractions, expansions).

Rough design guidelines are given in building service engineering standards [2] in order to calculate and reduce the resistance of the above-listed elements, however, researchers are constantly investigating more elaborate geometries for further energetic improvement. Examples of the scientific literature given in the following are all related to the field of mechanical ventilation. In order to reduce the flow resistance of an elbow, Ziganshin et al. [3] provided a novel geometry with a profiled internal wall, which also significantly shortened the influence zone of the element. Yin et al. [4] and Zhang et al. [5] both investigated the effect of guide vanes mounted in an elbow: the former paper reports a computational fluid dynamics (CFD) based optimization process of the geometry and location of the guide vanes, using field synergy and viscous dissipation principles, while the latter one investigates

Cite this article as: Lukács, E., Vad, J. "Parameter Study of a Loss Reducing Passive Flow Control Method in a Square-to-square Sudden Expansion", Periodica Polytechnica Mechanical Engineering, 67(3), pp. 204–213, 2023. https://doi.org/10.3311/PPme.22389

the loss reducing capabilities of a guide vane with a saw-like trailing edge, designed using biomimetic principles, inspired by the wings of bats and the fins of humpback whales. As for T-junctions, biomimicry has as well been taken advantage of by Gao et al. [6] to propose a novel shape – resembling tree junctions – with decreased losses. The same group of researchers also provided a CFD-based optimization for the location and shape of a guide vane in order to minimize the losses of tees [7].

Regarding changing the cross-section of ducts, expansions generally represent a higher hydraulic resistance than contractions [8]. Properly designed diffusers can expand the area with moderate losses, however, due to the generally limited available space in the building industry, often much shorter sudden expansions get to be installed [9]. Scientific literature on the resistance reduction of sudden expansions, however, is limited to axisymmetric cases: Heskestad [10], e.g., applies a suction at the step edge, while Mandal et al. [11] investigate the effect of a fence placed inside the separation zone. Bae and Kim [12, 13] report an extensive CFD-based parameter study of a sudden expansion with a chamfered edge, being analogous to the stepped diffuser geometry described by Idelchik [8]. So as a start to fill in the gap regarding the loss reduction of rectangular expansions, the authors of the present article offered a simple, passive flow control technique for square-to-square sudden expansions in [14]. Loss-reducing appendages – aka miniflaps – were placed at the edge of the step, and an experimental campaign was carried out as a proof of concept for a concentric, square-to-square sudden expansion of an area-ratio of $n_{AR} = (d_{h2}/d_{h1})^2 = 2.78$ and a miniflap length of $l_{mf} = 0.13 d_{h1}$ (for the sketch of the geometry and the notations, see Fig. 1 (a)). A 14–25% relative reduction of the loss coefficient could be reached for the investigated Reynolds number range of $\mathrm{Re} = (0.37 - 1.82) \cdot 10^5$. The optimum angle of the miniflaps resulted to be $\alpha_{opt} = 12° \pm 1°$, demonstrating only a minor dependence on the Reynolds number. The experiments, however, were confined to only one investigated geometry, hence a need to expand the parameter space was conceived by the authors.

CFD simulations have been proven to be an effective and economically affordable tool to expand the parameter range and get a deeper insight into flow details, sometimes unavailable from measurement results. Although numerical simulations generally come at a lower cost than experiments, the number of the examined parameters – consequently the number of simulation cases – should be strongly

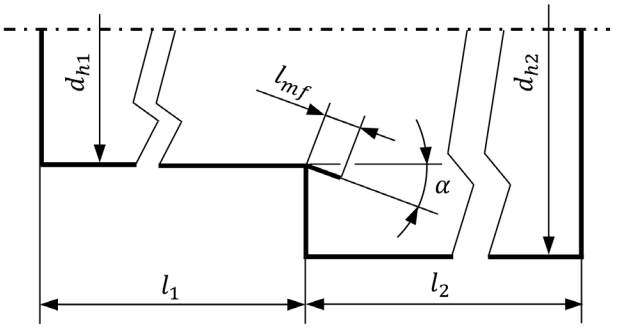

(a)

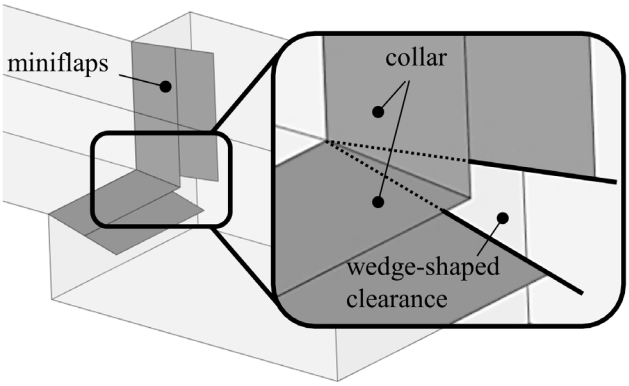

(b)

Fig. 1 Geometry of the sudden expansion equipped with miniflaps; (a) Sketch and notations; (b) 3D representation of the quarter geometry with the collar

controlled to keep the need for computational resources and time at a moderate level. However, basic trends and sensitivity of the loss coefficient to the different parameters are expected to be predicted from even a limited number of simulations, which can also give a fundamental indication for expanding the parameter range in the framework of future research. To this end, this study provides a modest expansion of the parameter space with the help of CFD, as given in Table 1. The area ratio is examined in the practically relevant range, while the miniflap angles are set in the proximity of the expected optimum [14]. As the geometry appearing in the formerly cited research of Bae and Kim [12, 13] shares some common features with the miniflap method, their results provide guidelines in the current study for setting the miniflap length range, provided in terms of the upstream hydraulic diameter.

Table 1 Numerically investigated parameter space

	1	2	3
Area ratio (n_{AR})	2	2.78	4
Miniflap length (l_{mf}/d_{h1})	0.13	0.3	0.5
Miniflap angle (α)	9	12	15
Reynolds number (Re)	$1.08 \cdot 10^5$		

The dependence of the optimum angle on the Reynolds number is expected to be modest [12–14], therefore, only one Reynolds number is examined. The Reynolds number is defined as $\mathrm{Re} = \bar{u}_1 d_{h1}/\nu$, where $\bar{u}_1$ is the average upstream streamwise velocity, d_{h1} is the upstream hydraulic diameter, and ν is the kinematic viscosity of air.

Based on the numerical results, the research aims at predicting a trend of:

1. the optimal miniflap angle in the function of the miniflap length and the area ratio;
2. the loss coefficient at the optimal angle of the miniflap in the function of the miniflap length and area ratio.

2 Methods

The numerical procedure presented in this paper has been carried out using the ANSYS Workbench 2021 R2 commercial CFD software package [15].

2.1 Geometry

The sketch of the numerical model of the sudden expansion with the miniflaps is demonstrated in Fig. 1 (a). The upstream and downstream duct lengths and inner hydraulic diameters are denoted as l_1, l_2, d_{h1} and d_{h2}, respectively, while l_{mf} stands for the length of the miniflaps, and α stands for the angle of the miniflaps with respect to the duct axis. A total of 27 different geometry variants are presented in the current study, as it has been given earlier in Table 1. The geometries have been created by ANSYS DesignModeler, allowing for easy parametrization.

As former measurements have demonstrated that the flow is fairly symmetrical [9, 14], only a quarter channel is used for the present parameter study in order to reduce the size of the numerical mesh, thus the time needed for the simulations. The upstream duct length ($l_1 = 5d_{h1}$) has been set to be long enough to avoid any possible upstream effect of the sudden expansion [16], while the downstream length ($l_2 = 10d_{h2}$) is chosen to be long enough to allow for sufficient flow relaxation, thus determining the loss coefficient with low uncertainty. The adequacy of the utilized downstream length has been confirmed by additional CFD studies for $l_2 = 46d_{h2}$. As for the miniflaps, two simplifications of the real geometry were applied in order to enable the creation of a numerical mesh that is of sufficiently high quality for the numerical method to converge:

1. the miniflaps were modeled as infinitely thin walls;
2. a short collar – basically a short section of a pyramidal diffuser – was added to the geometry, closing the wedge-shaped clearance between the miniflaps, as highlighted in Fig. 1 (b).

It is important to note that the extent of the collar appears exaggerated in Fig. 1 for better visibility. However, the effective length of the collar was only 10% of the shortest miniflap length, and it remained constant throughout the entire examined parameter range.

2.2 Mesh and boundary conditions

A 3D mesh – shown in Fig. 2 – consisting of purely hexahedral elements was generated with the MultiZone method of the ANSYS Meshing program. The mesh was refined by setting the bias factor in the proximity of the step edge, in the free shear layer forming at the trailing edge of the miniflap, and in the boundary layers. The dimensionless wall distance $y+$ was controlled to be around 1 for an appropriate resolution of the viscous sublayer.

A mesh independence study was carried out for the representative case of $n_{AR} = 2.78$; $l_{mf} = 0.13d_{h1}$; $\alpha = 12°$; $\mathrm{Re} = 1.08 \cdot 10^5$. The estimated uncertainty of the loss coefficient due to the discretization error was determined using the Grid Convergence Index (GCI) method [17]. The mesh metrics, predicted loss coefficient values, and their estimated discretization errors, with respect to the extrapolated case, are summarized in Table 2. Based on the mesh independence study, the medium-sized mesh with $2.08 \cdot 10^6$ elements was accepted, for which the estimated relative discretization error is below 1%. The basic meshing setup parameters were kept the same in the case of all other geometry variants.

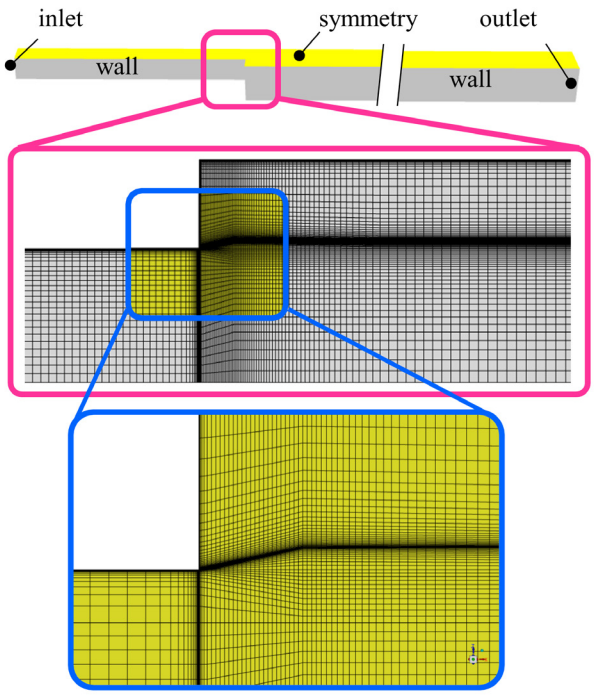

Fig. 2 Numerical mesh and boundary conditions for a representative geometry of $n_{AR} = 2.78$; $l_{mf} = 0.13d_{h1}$; $\alpha = 12°$

Table 2 Mesh independence study

Number of cells	Loss coefficient	Relative error
$1.02 \cdot 10^6$	0.358	2.71%
$2.08 \cdot 10^6$	0.363	0.98%
$4.26 \cdot 10^6$	0.365	0.40%
extrapolated	0.366	-

Boundary conditions were applied to the numerical model as depicted in Fig. 2: velocity inlet on the inlet surface, pressure outlet (0 gauge pressure) on the outlet surface, symmetry on the two planes of symmetry and no-slip, smooth wall on the duct and miniflap walls. Considering the inlet velocity, fully developed flow profiles were obtained from auxiliary simulations in short square ducts, applying periodic inlet-outlet boundary conditions [18].

2.3 Numerical method

The numerical simulations have been carried out with the ANSYS Fluent software, which solves the Reynolds-averaged continuity and Navier-Stokes equations for a steady-state, turbulent flow. The working fluid was incompressible air, thus the pressure-based solver was used. As for the turbulence model, the generalized *k-ω* (GEKO) model was chosen, for which the selection procedure is explained later in Section 3.1. The coupled solution scheme was applied for the pressure-velocity coupling, and second-order upwinding was set for every flux formulation. All simulations were run until iterative convergence was reached. Convergence was determined by a decrease of at least 4 orders of magnitude in the continuity residual, and a decrease of at least 6 orders of magnitude in the residuals for velocity and turbulence components. Additionally, physical properties such as the mass-weighted average of the total pressure on the inlet and outlet, and local streamwise and cross-stream velocities in control points located close downstream of the step in the shear layer were also monitored. Convergence was assessed when these values reached a nearly constant value. As a separated flow is inherently unsteady, the residuals and the monitored physical properties displayed minor oscillations in some cases. Although the amplitude of these oscillations remained below 0.01% for the mass-weighted average of inlet and outlet total pressures, steady statistics data sampling was performed for 4–6 cycles to eliminate uncertainty in the calculated loss coefficient that might originate from using a random instantaneous value of the inlet and outlet total pressures.

2.4 The loss coefficient

The loss coefficient of any hydraulic element is defined as the total pressure drop introduced by the element, divided by the relevant – generally upstream – dynamic pressure. As for determining the loss coefficient of a sudden expansion, the authors have come across three slightly different ways of evaluation encountered in the scientific literature, depending on the applied method of evaluation:

1. the *extrapolation method* [12, 13, 16];
2. *maximum pressure* method [9, 10, 14];
3. *semi-empirical method* [8, 9]. These three approaches are briefly described below.

For the *extrapolation method*, the mass-weighted average of the total pressure needs to be evaluated at the inlet and outlet of the investigated duct section, that both lie sufficiently far from the element in question to avoid any upstream effects and to ensure enough downstream length for the flow to reach a completely developed state. The additional duct sections, however, introduce additional frictional losses into the system that need to be eliminated from the equation of the loss coefficient of the sudden expansion. A generally accepted method to carry out this elimination is to simply subtract the friction losses, calculated for a fully developed flow, from the total pressure difference, thus, both the local and the frictional losses introduced by the element in question will be inherently included in the calculated loss coefficient. Accordingly, the loss coefficient of the sudden expansion is calculated as shown in Eqs. (1)–(4):

$$\zeta_{ext} = \frac{\Delta p_{tot} - \left(\Delta p_{fr,1} + \Delta p_{fr,2}\right)}{\frac{\rho}{2}\bar{u}_1^2}, \tag{1}$$

$$\Delta p_{fr} = \lambda \frac{l}{d_h} \cdot \frac{\rho}{2}\bar{u}^2, \tag{2}$$

$$\frac{1}{\sqrt{\lambda}} = 2 \cdot \log\left(\mathrm{Re}\sqrt{\lambda}\right) - 0.8, \tag{3}$$

$$\mathrm{Re}_1 = \frac{\bar{u} d_h}{\nu}, \tag{4}$$

where ζ_{ext} is the loss coefficient calculated using the *extrapolation method*, Δp_{tot} is the difference of the mass-weighted average of the inlet and outlet total pressures, Δp_{fr} is the friction loss of the straight duct in case of a fully developed

flow, where subscript 1 and 2 stand for the upstream and downstream duct sections, respectively, ρ is the density of air, $\bar{u}$ is the area-averaged streamwise velocity, λ is the pipe friction coefficient, l is the duct length, d_h is the hydraulic diameter, Re is the Reynolds number, and ν is the kinematic viscosity of air. Equation (3) is generally referred to as the Kármán-Prandtl equation to calculate the pipe friction coefficient and has been shown to be valid for hydraulically smooth ducts of square cross-sections as well [8].

Equations (5)–(7) show the calculation process of the *maximum pressure method*, where the loss coefficient ($\zeta_{\max p}$) is determined based on the difference of the ideal static pressure increase (Δp_{id}) and the effective static pressure increase (Δp_{eff}). The ideal static pressure increase (Eq. (6)) is derived from the Bernoulli equation for a fully developed flow, while the effective static pressure increase (Eq. (7)) is determined as the difference between the maximum wall static pressure downstream ($p_{\max}$) and a reference wall static pressure upstream of the expansion (p_{ref}), located close – at a distance of $d_{h1}/3$ in the reference experiments [14] – to the step of the sudden expansion.

$$\zeta_{\max p} = \frac{\Delta p_{id} - \Delta p_{real}}{\frac{\rho}{2}\bar{u}_1^2} \tag{5}$$

$$\Delta p_{id} = N \cdot \frac{\rho}{2}\bar{u}_1^2 \left(1 - \frac{1}{n_{AR}^2}\right) \tag{6}$$

$$\Delta p_{eff} = p_{\max} - p_{ref} \tag{7}$$

The term N, appearing in Eq. (6), is the so-called energy coefficient, accounting implicitly for the fully developed flow profile. Its detailed calculation is not shown in here for conciseness but is thoroughly explained in [8, 9]. Although the maximum pressure method neglects the effect of change in pipe friction in relation to the case of a fully developed flow, its practical relevance is unquestionable, regarding that a significantly shorter downstream duct section is needed than in the case of the extrapolation method. The applicability of the maximum pressure method is addressed in Section 3.2.

The semi-empirical method is based on predicting the real pressure increase, appearing in Eq. (5), with the help of the momentum theorem. The formula for estimating the loss of a sudden expansion in the case of a fully developed inlet velocity distribution (ζ_{emp}) is shown in Eq. (8), in which M is the momentum coefficient [8, 9]. The applicability of Eq. (8) in the case of square-to-square sudden expansions was confirmed, and a detailed description of the calculation procedure is given in [9].

$$\zeta_{emp} = N - \frac{2M}{n_{AR}} + \frac{2M - N}{n_{AR}^2} \tag{8}$$

2.5 Static pressure regain

Although the present research focuses on the reduction of the loss coefficient, an interesting theoretical supplement is given herein briefly about another important characteristic of the expansions in general, the static pressure regain, describing the ability of the expansion to maximize the available static pressure downstream of the element. It is interesting to note that while design criteria for maximizing the static pressure regain of diffusers is given in detail, e.g., in [8], the discussion of sudden expansions seems to be underrepresented by the scientific literature from this point of view, despite the possibility of its easy analytical treatment, described in the followings. The effective pressure rise, discussed in Section 2.4, may not only be determined by measurement but it can also be expressed by semi-empirical means from the momentum equation, presuming uniform and incompressible flow. The classic formula for the effective pressure rise ($\Delta p_{eff,emp}$) is shown by Eq. (9), as available in the literature [19]. Its nondimensionalized form is termed the static pressure regain coefficient ($c_{p,eff,emp}$), and is given in Eq. (10).

$$\Delta p_{eff,emp} = \rho \bar{u}_1^2 \left(\frac{1}{n_{AR}} - \frac{1}{n_{AR}^2}\right) \tag{9}$$

$$c_{p,eff,emp} = \frac{\Delta p_{eff,emp}}{\frac{\rho}{2}\bar{u}_1^2} = \frac{2\left(n_{AR} - 1\right)}{n_{AR}^2} \tag{10}$$

The above formula in Eq. (10) offers a simple and effective approximate tool for analysis of the operation of a sudden expansion. As has been pointed out by the present authors in an extreme value calculation, via partial differentiation of the formula with respect to n_{AR}, a maximum static pressure rise is expected at $n_{AR} = 2$. The adequacy of this analytical result is supported by experimental data in [20].

3 Results and discussion

3.1 Turbulence model

The success of a numerical simulation is predetermined by the selection of the appropriate turbulence model that fits the flow scenario to be modeled the best. In the present case

of a square-to-square sudden expansion, one has to keep in mind that secondary flow of the second kind is present in non-circular ducts, even when the flow is fully developed [21]. As discussed in [18], besides the scale-resolving models – which have a prohibitive price for the present parameter study – two turbulent model families can be taken into account for the present case: the Reynolds stress and the *k*-*ω* based models. As the authors have faced unresolvable convergence issues with the Reynolds stress model – which is even mentioned as a main shortcoming of the turbulence model in the software manual – therefore they were to keep at the *k*-*ω* model family, from which the GEKO model was chosen due to its favorable properties, described in the followings.

The GEKO is a relatively new turbulence model, aiming at the consolidation of the numerous different turbulence models [22]. With its six freely adjustable parameters, the user can tune the model to various different flow scenarios without ruining the basic calibration schemes, such as the development of a boundary layer over a flat plate. The default parameter setup is an exact formulation of the *k*-*ω* SST model. A short description of the two most relevant adjustable parameters is given in this document, while a more detailed specification, together with the formulation equations, can be found in [22]:

1. The corner coefficient (C_{corner}) is a non-linear stress-strain term that is able to account for the secondary flows developing in non-circular ducts. The adjustment of this parameter was carried out by one of the authors of the present study for a straight square duct [18] and was recommended to take the value of $C_{corner} = 0.9$. The results presented in [18] are briefly summarized in Section 3.2.
2. The separation coefficient (C_{sep}) is responsible for the prediction of the onset of separation. Increasing its value leads to a decreased eddy-viscosity, thus an earlier flow separation in the presence of an adverse pressure gradient. The adjustment of this parameter is crucial in order to predict the optimum angle of the miniflaps, and is presented in Section 3.2.

3.2 Validation

The adjustment of the corner coefficient was conducted by validating the CFD results against laser-Doppler anemometer velocity measurements in a straight square duct, for a fully developed flow at Re = $0.36 \cdot 10^5$. The results are presented in Fig. 3. Fig. 3 (a) highlights the evaluation

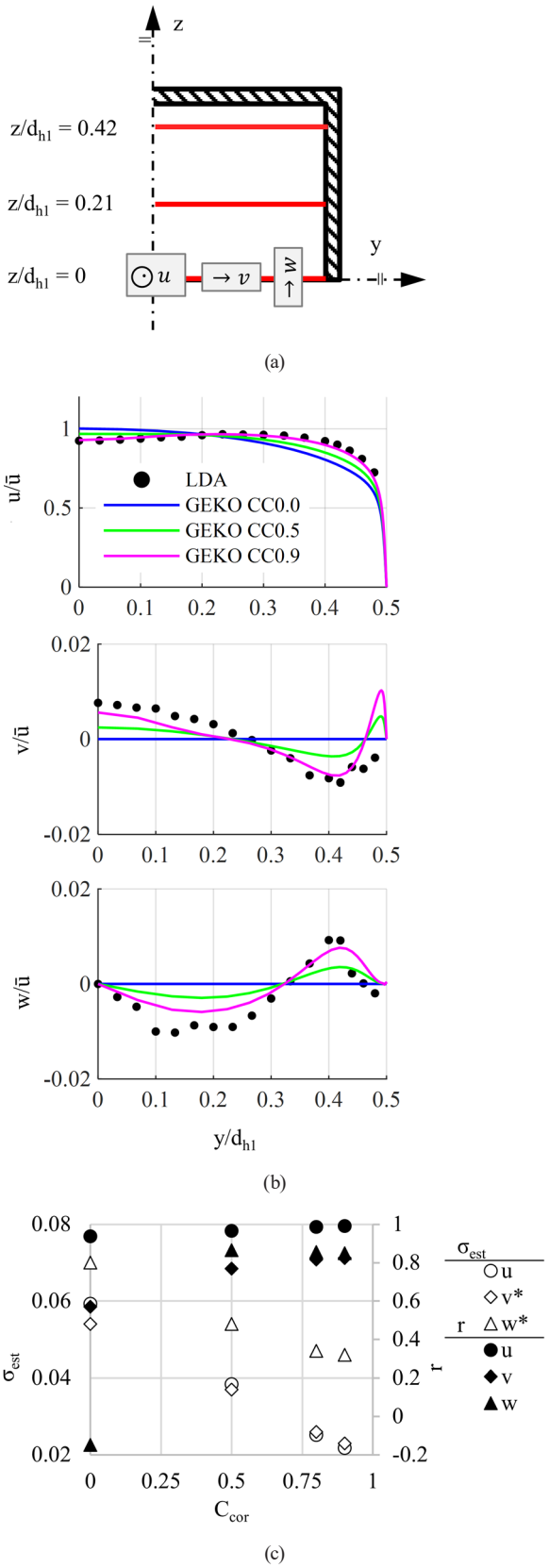

Fig. 3 Validation of the CFD results – velocity field; (a) Validation profiles and notation; (b) Velocity components at $z/d_{h1} = 0.42$; (c) Adjustment of the corner coefficient: $d_{h1} = 150$ mm; $\bar{u} = 3.78$ m/s

profiles located at $z/d_{h1} = 0$; 0.21; 0.42, along with the coordinate system and the notation of the velocity components. Fig. 3 (b) displays the dimensionless velocity profiles at a representative location of $z/d_{h1} = 0.42$ for various C_{cor} values, where the number in GEKO CC0.9 appearing in the legend corresponds to the value of C_{cor}. Finally, Fig. 3 (c) provides the quantitative and qualitative assessment of the validation process for all profiles ($z/d_{h1} = 0$; 0.21; 0.42), for which the standard error of the estimate (σ_{est}) and the sample Pearson correlation coefficient (r) were determined by Eq. (11) and Eq. (12), respectively. It is important to note that the standard error of the estimate was evaluated for multiple profiles collectively, yielding a single σ_{est} value that represents the overall discrepancy between the experimental and numerical results for the entire flow field. On the other hand, the correlation coefficients hold significance only when determined for each examined profile individually. Therefore, they have been computed separately for each profile, and their average value is reported here (Eqs. (11) and (12)):

$$\sigma_{est} = \sqrt{\frac{\sum_{i=1}^{n}\left(\varphi_{exp,i} - \varphi_{\mathrm{CFD},i}\right)^2}{n}}, \tag{11}$$

$$r = \frac{\sum_{i=1}^{n}\left(\varphi_{exp,i} - \bar{\varphi}_{exp}\right)\left(\varphi_{\mathrm{CFD},i} - \bar{\varphi}_{\mathrm{CFD}}\right)}{\sqrt{\sum_{i=1}^{n}\left(\varphi_{exp,i} - \bar{\varphi}_{exp}\right)^2}\sqrt{\sum_{i=1}^{n}\left(\varphi_{\mathrm{CFD},i} - \bar{\varphi}_{\mathrm{CFD}}\right)^2}}, \tag{12}$$

where φ_i is the examined variable at a sample point i, $\bar{\varphi}$ is the arithmetic mean of the variable, and n is the number of sample points. The subscripts *exp* and CFD stand for the experimentally and numerically determined values.

The optimal setting of the corner coefficient is found where σ_{est} is minimal, and r is maximal. Thus it can be concluded from Fig. 3 (c) that the performance of the GEKO model is significantly improving for all examined variables as the corner coefficient increases. This observation is also corroborated by the velocity profiles in Fig. 3 (b), where the GEKO $C_{cor} = 0.9$ simulation is notably in better agreement with the measurement results than the GEKO $C_{cor} = 0$. As expected, $C_{cor} = 0$ fails to model the secondary flows, resulting in predicted cross-stream velocities of zero. However, as the value of C_{cor} increases, the model successfully induces the secondary flow of the second kind. It is important to note that raising the corner coefficient above 0.9 leads to a non-physical asymmetry in the flow, which observation is also emphasized by the creators of the GEKO model in [22]. In order to avoid this non-physical asymmetry, the value of C_{cor} was maximized at 0.9 during the present research.

For validation of the numerical results and adjustment of the separation coefficient, the numerical and experimental loss coefficients in the function of the miniflap angle have been compared, for $n_{AR} = 2.78$; $l_{mf} = 0.13 d_{h1}$; $\alpha = 0°$–$21°$ and $\mathrm{Re} = 1.08 \cdot 10^5$. The results are shown in Fig. 4, where the number in GEKO CS1.75, appearing in the legend, stands for the value of C_{sep}. The experimental loss coefficients, given in [14], were determined using the *maximum pressure method*; the detailed description of the experimental setup and the process of evaluation is given therein. For the sake of a like-for-like comparison, the numerical loss coefficients appearing in Fig. 4 (a) were evaluated the same way (except for GEKO 1 (ext), where the *extrapolation method* was used). For a quantitative and qualitative comparison of the CFD and experimental results, σ_{est} and r are shown in Fig. 4 (b). The separation coefficient was studied for $C_{sep} = 0.7$; 1.0; 1.5; 1.75, where the two extrema are the minimum and maximum allowed values of the coefficient [22].

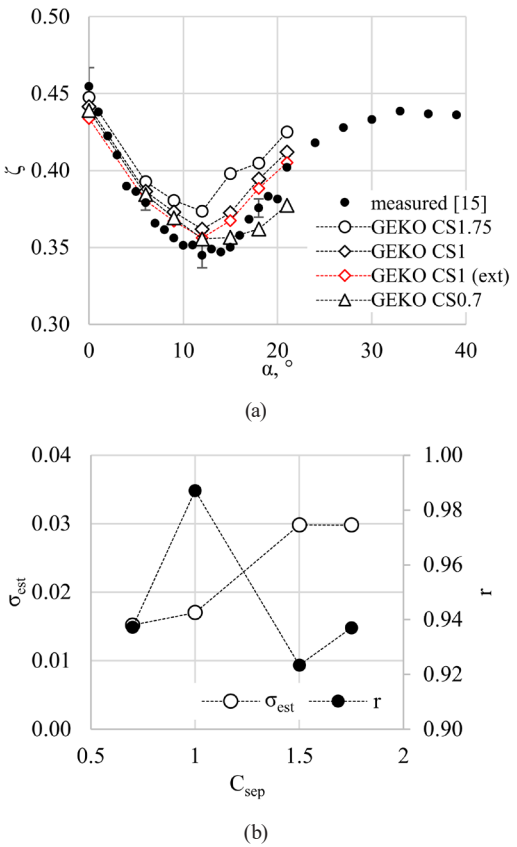

Fig. 4 Validation of the CFD results – loss coefficient; (a) Loss coefficient in the function of the miniflap angle; (b) Adjustment of the separation coefficient

As it was described in the case of the corner coefficient, the optimal setting of the separation coefficient is found where σ_{est} is minimal, and r is maximal. As it can be seen in Fig. 4 (b), this requirement is fulfilled for σ_{est} at $C_{sep} = 0.7$, while for r at $C_{sep} = 1.0$. However, the use of $C_{sep} = 0.7$ can easily lead to the underseparation of the boundary layer from the miniflap surface [22], also indicated by the fact that the slope of the $C_{sep} = 0.7$ curve in Fig. 4 (a) is significantly smaller than that of the experimental results in the $\alpha = 12°–21°$ range. Should the $C_{sep} = 0.7$ curve be extrapolated towards higher values of the miniflap angle, both coefficients would be expected to notably deteriorate. That being said, the authors preferred setting the separation coefficient value to $C_{sep} = 1.0$.

Commenting on the validity of the CFD results, it can be observed in Fig. 4 (a) that the loss coefficient is overestimated by the numerical method for the practically relevant range of $\alpha = 6°–18°$ by 4–6%, however, the correlation – for $C_{sep} = 1.0$ – is excellent. The loss coefficients have also been calculated by the *extrapolation method*, and the results are depicted for $C_{sep} = 1.0$ in Fig. 3 (a) in red. Although ζ_{ext} is persistently smaller than $\zeta_{max p}$, this difference remains within the expected measurement uncertainty, being only 1–2%. As such, even in situations where limitations in the axial extent of the experimental setup or the numerical model prevent the use of the *extrapolation method*, the *maximum pressure method* still yields sufficiently accurate results.

3.3 Parameter study

There are two practically important pieces of information that need to be retrieved from the results of the numerical simulations for the expanded parameter range:

1. the optimum angle of the miniflaps for a given miniflap length and area ratio in order to minimize the loss coefficient;
2. the value of the loss coefficient in the function of the miniflap length for a given area ratio when the miniflaps are set to an optimal angle.

Fig. 5 shows the loss coefficient in the function of the miniflap angle for all examined miniflap length and area ratios of the sudden expansion. For certain cases, the local minimum at $\alpha = 12°$ is very definite, while for other cases – typically for the two smaller area ratios and the two longer miniflap lengths – the curves are very flat in the $\alpha = 9°–12°$ range. However, based on the measurement and validation results in Fig. 4 (a), a parabolic nature of the loss coefficient in the proximity of the optimum angle is

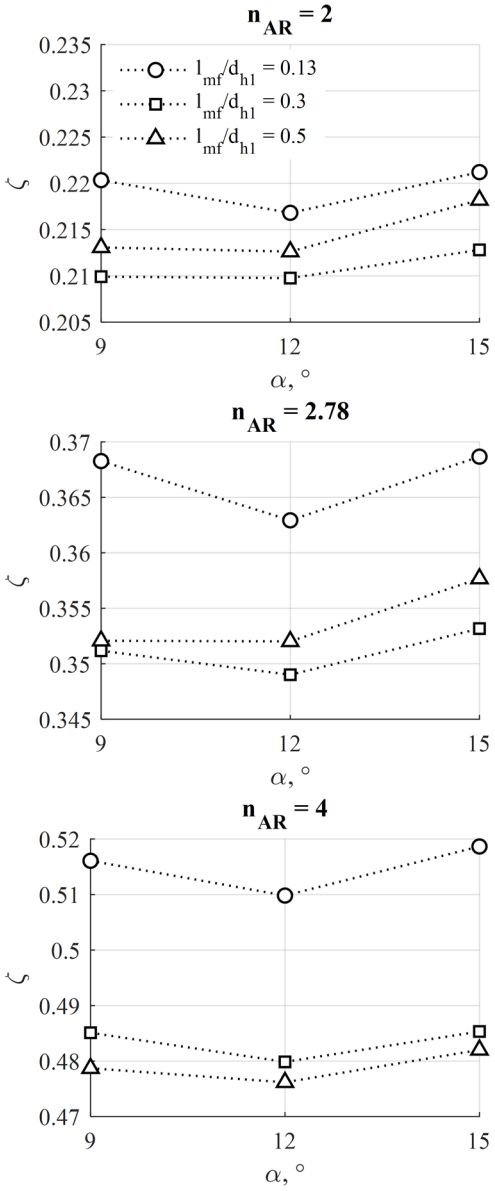

Fig. 5 Loss coefficient of the sudden expansion equipped with miniflaps in the function of the miniflap angle, for $n_{AR} = 2$; 2.78; 4; $l_{mf} = 0.13d_{h1}$ (20 mm); $0.3d_{h1}$ (45 mm); $0.5d_{h1}$ (75 mm); $d_{h1} = 150$ mm

expected, which suggests that the minimum loss coefficient is going to fall in the $\alpha = 9°–12°$ range, for all presently examined cases. In order to localize the minima of the ζ versus α curves more precisely, it is strongly advised to broaden the investigated miniflap angles to a range of $\alpha = 6°–15°$ during the course of a future study.

It is also observable in Fig. 5 that the loss coefficient in the case of $n_{AR} = 2$; 2.78, the miniflaps of length $0.5d_{h1}$ cause larger losses than the ones with $0.3d_{h1}$. This trend is more clearly demonstrated in Fig. 6, where ζ_{min}/ζ_{emp} is plotted against the dimensionless miniflap length, ζ_{min} denoting the minimum value of the loss coefficient for a given area ratio and miniflap length, and ζ_{emp} standing for the empirical

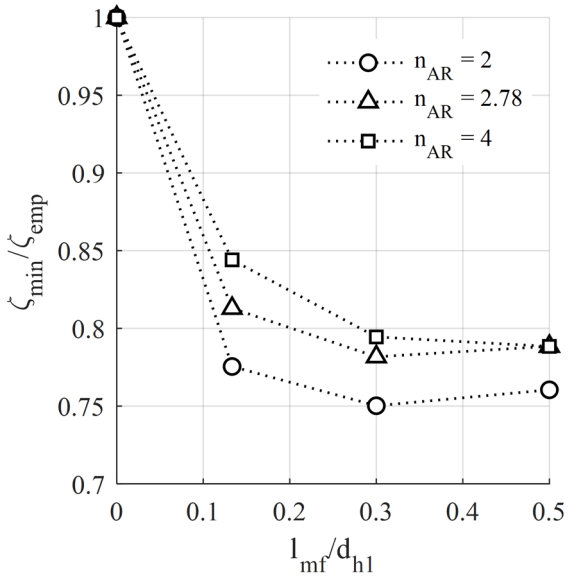

Fig. 6 Impact of the miniflap length on the loss coefficient; d_{h1} = 150 mm

loss coefficient of the sudden expansion without miniflaps (Eq. (8)). The calculated curves show a degressive trend for all area ratios. It can also be observed that for the two smaller area ratios, there is a local minimum at $l_{mf} = 0.3d_{h1}$, while in the case of $n_{AR} = 4$, the loss coefficient is continuously decreasing up to $l_{mf} = 0.5d_{h1}$, although no significant further improvement is reached between $l_{mf} = (0.3–0.5)d_{h1}$. Based on Fig. 6, it can be concluded that the miniflaps are able to reduce the loss coefficient of sudden expansions in the examined parameter range by a maximum of ~20–25% at a miniflap length of around $l_{mf} = 0.3d_{h1}$.

4 Conclusion

In this paper, a confined parameter study was carried out by means of CFD for a passive flow control method, aiming at the reduction of the loss coefficient of square-to-square sudden expansions. A proof of concept was given by experimental means for one single sudden expansion and miniflap geometry in [14]. In the present study, the parameter space has been extended with respect to [14], considering the area ratio of the sudden expansion and the miniflap length. The applied turbulence model was the generalized k-ω model, for which the separation coefficient has been adjusted with the help of the measurement results in [14].

The numerical results showed that the optimum miniflap angle setup, belonging to the smallest loss coefficient, is expected to fall between α = 9°–12°, displaying only a minor dependence on the area ratio and the miniflap length. For more detailed information on optimal angle setup, the examined parameter range is advised to be extended to at least α = 6°–18°. As for the miniflap length, the loss coefficient was shown to be decreased by ~20–25% up to a miniflap length of $0.3d_{h1}$, beyond which length the loss coefficient stayed nearly constant or even slightly increased in the case of the smaller area ratios. Therefore, the presently investigated miniflap length range of $(0.3–0.5)d_{h1}$ is expected to be adequately ample for the currently studied area ratio but might need to be expanded in case larger area ratios should be examined.

Besides widening the investigated miniflap angle range, future studies should also concentrate on extending the Reynolds number and the area ratio range, which exceeded the framework of the present research. The authors preserve priority to fit empirical correlation functions to the points of the dataset in order to quantitatively aid the design of miniflaps.

Acknowledgement

Project no. TKP-6-6/PALY-2021 has been implemented with the support provided by the Ministry of Culture and Innovation of Hungary from the National Research, Development and Innovation Fund, financed under the TKP2021-NVA funding scheme.

References

[1] Pérez-Lombard, L., Ortiz, J., Pout, C. "A review on buildings energy consumption information", Energy and Buildings, 40(3), pp. 394–398, 2008. https://doi.org/10.1016/j.enbuild.2007.03.007

[2] European Committee for Standardization "EN 1505:1997 Ventilation for buildings. Sheet metal air ducts and fittings with rectangular cross section. Dimensions", European Committee for Standardization , Brussels, Belgium, 1997.

[3] Ziganshin, A. M., Beljaeva, E. E., Logachev, K. I., Averkova, O. A. "Decrease of pressure losses in elbow fittings of ventilation systems of thermal power plant buildings", IOP Conference Series: Earth and Environmental Science, 288, 012133, 2019. https://doi.org/10.1088/1755-1315/288/1/012133

[4] Yin, Y., Li, A., Wen, X., Zhang, J., Zhang, X., Guo, J., Li, J., Zhang, W., Che, J. "Resistance reduction of an elbow with a guide vane based on the field synergy principle and viscous dissipation analysis", Journal of Building Engineering, 54, 104649, 2022. https://doi.org/10.1016/j.jobe.2022.104649

[5] Zhang, C., Li, A., Che, J., Li, Y., Liu, Q., Zhao Y. "A low-resistance elbow with a bionic sawtooth guide vane in ventilation and air conditioning systems", Building Simulation, 15(1), pp. 117–128, 2022. https://doi.org/10.1007/s12273-021-0782-y

[6] Gao, R., Liu, K., Li, A., Fang, Z., Yang, Z., Cong, B. "Biomimetic duct tee for reducing the local resistance of a ventilation and air-conditioning system", Building and Environment, 129, pp. 130–141, 2018. https://doi.org/10.1016/j.buildenv.2017.11.023

[7] Gao, R., Liu, K., Li, A., Fang, Z., Yang, Z., Cong, B. "Study of the shape optimization of a tee guide vane in a ventilation and air-conditioning duct", Building and Environment, 132, pp. 345–356, 2018. https://doi.org/10.1016/j.buildenv.2018.02.006

[8] Idelchik, I. E. "Handbook of Hydraulic Resistance", Jaico Publishing House, 2008. ISBN 978-1-56700-251-5

[9] Lukács, E., Vad, J. "Flow topology and loss analysis of a square-to-square sudden expansion relevant to HVAC systems: A case study", Journal of Building Engineering, 41, 102802, 2021. https://doi.org/10.1016/j.jobe.2021.102802

[10] Heskestad, G. "A suction scheme applied to flow through sudden enlargement", Journal of Basic Engineering, 90(4), pp. 541–552, 1968. https://doi.org/10.1115/1.3605188

[11] Mandal, D. K., Bandyopadhyay, S., Chakrabarti, S. "A numerical study on the flow through a plane symmetric sudden expansion with a fence viewed as a diffuser", International Journal of Engineering, Science and Technology, 3(8), pp. 210–233, 2011. https://doi.org/10.4314/ijest.v3i8.18

[12] Bae, Y., Kim, Y. I. "Prediction of local pressure drop for turbulent flow in axisymmetric sudden expansions with chamfered edge", Chemical Engineering Research and Design, 92(2), pp. 229–239, 2014. https://doi.org/10.1016/j.cherd.2013.07.016

[13] Bae, Y., Kim, Y. I. "Prediction of local loss coefficient for turbulent flow in axisymmetric sudden expansions with a chamfer: Effect of Reynolds number", Annals of Nuclear Energy, 73, pp. 33–38, 2014. https://doi.org/10.1016/j.anucene.2014.06.032

[14] Lukács, E., Vad, J. "A passive loss reduction method of square-to-square sudden expansions", Energy and Buildings, 266, 112113, 2022. https://doi.org/10.1016/j.enbuild.2022.112113

[15] ANSYS, Inc. "ANSYS Workbench (2021 R2)", [computer program] Ansys, Canonsburg, PA, USA, 2021.

[16] Tomor, A., Mervay, B., Kristóf, G. "Continuous Parametrization of Hydraulic Losses Caused by Diameter Transition in Cylindrical Pipes", In: Proceedings of the 5th International Scientific Conference on Advances in Mechanical Engineering, Debrecen, Hungary, 2017, pp. 581–587. ISBN 978-963-473-304-1

[17] Celik, I. B., Ghia, U., Roache, P. J., Freitas, C. J. "Procedure for Estimation and Reporting of Uncertainty Due to Discretization in CFD Applications", Journal of Fluids Engineering – Transactions of the ASME, 130(7), 078001, 2008. https://doi.org/10.1115/1.2960953

[18] Lukács, E. "Turbulens áramlás numerikus szimulációja négyzet keresztmetszetű csatornában" (Numerical simulation of turbulent flow in a duct of square cross-section), In: Tavaszi Szél 2022 / Spring Wind 2022 II., Pécs, Hungary, 2022, pp. 423–438. ISBN 978-615-6457-13-4 (in Hungarian)

[19] Gerhart, M. T., Gross, R. J. "Fundamentals of Fluid Mechanics", Addison-Wesley Publishing Company, 1985. ISBN 9780201114102

[20] Benedict, R. P., Carlucci, N. A., Swetz, S. D. "Flow losses in abrupt enlargements and contractions", Journal of Engineering for Gas Turbines and Power, 88(1), pp. 79–81, 1966. https://doi.org/10.1115/1.3678482

[21] Pirozzoli, S., Modesti, D., Orlandi, P., Grasso, F. "Turbulence and secondary motions in square duct flow", Journal of Fluid Mechanics, 840, pp. 631–655, 2018. https://doi.org/10.1017/jfm.2018.66

[22] Menter, F., Lechner, R., Matyushenko, A. "Best Practice: Generalized k-ω Two-Equation Turbulence Model in ANSYS CFD (GEKO)", Technical report ANSYS, ANSYS Inc., Canonsburg, PA, USA, 2019.